

Behavior of plain concrete subjected to tensile loading at high strain-rate

E.Cadoni

Institute of Materials Mechanics, Lugano-Grancia, Switzerland

C.Albertini & K.Labibes

Dynalab, Ispra, Italy

G.Solomos

European Commission, Joint Research Centre, ISIS, Ispra, Italy

ABSTRACT: The results obtained during a testing program for tensile behavior over a large range of strain-rates (10^{-6} to 10 s $^{-1}$) are summarized in this paper. The tests have been performed on cube specimens of 200 mm and 60 mm sides with aggregates of 5, 10 and 25 mm size. The high strain-rate tests have been carried out using a large Hopkinson bar bundle equipment. The aim of this study was to produce new data on basic subject of industrial importance that is the behavior of plain concrete at the strain rates corresponding to those caused by quasi-static, earthquake and impact loading.

1 INTRODUCTION

In the recent years the discussion on strain-rate problem of concrete has been opened-up because of the increased use of normal and very high strength concrete in special structures as well as because of the several new fields of interest (from defensive structures to demolition of old buildings). However, due to the difficulty in the realization of tests, only few experimental data are available. For this reason a large scale experimental exercise on concrete subjected to dynamic load has been conceived using a new methodology.

For high strain-rate studies two experimental techniques are generally used: the technique of drop weight and that of Hopkinson bar. A variation of the latter technique, called the Hopkinson Bar Bundle (HBB) (Albertini et al. 1994, 1997, 1998, 1999), was used in this study. These results are part of a broader research program on the uniaxial dynamic behavior of concrete, developed in the context of the "Access to Large Scale Facilities" action of the Frame Work Program of the European Union.

The present paper describes experimental results of tensile tests of plain concrete at strain rates corresponding to those induced by quasi-static, earthquake and impact loading.

2 MATERIALS

For the concrete mix a crushed limestone aggregate, subdivided in 7 classes from powder to 25 mm maximum size, and a Portland cement (CEM I 42.5) were used.

The concrete has been characterized on the basis of several properties like rheological properties (workability of the fresh mix), mechanical properties (development of the strength in tension and compression), elastic properties (development of the static, dynamic and vibration elastic modulus) etc. Furthermore, fracture mechanics tests were performed to evaluate the fracture energy characteristics. The specimens for the general concrete characterization were cured in an accurately controlled environmental condition: 20°C and 95% R.H.

Table 1. Concrete Mix design

Components	(kg/m ³)
Aggregate	1880
Cement CEM I 42.5	395
Superplasticizer	6.5
Water	201
Volumetric mass	2482

The concrete mechanical characteristics were evaluated as follows:

- the static elastic modulus (SEM) was evaluated on 3 prisms 15x15x60 cm³ measuring by LVDT the strain in loading cycles between 0.5 and 5 MPa. Furthermore, the vibration (VEM) and dynamic elastic modulus (DEM) was also evaluated on 16x16x48 cm³ prisms by means of ultrasonic wave propagation and resonance frequency in bending condition respectively.
- the compressive cubic strengths were evaluated after 28 days on cubic specimen 15 cm in side, carried out with a loading rate of 0.50 MPa/s.
- the fracture energy and the flexural tensile stress were obtained by three point bending test on

(10x10x84 cm³) notched prisms, following the RILEM recommendation.

The average properties of concrete were as follows:

Static elastic modulus	43.1 GPa
Dynamic elastic modulus	54.8 GPa
Vibration elastic modulus	41.4 GPa
Compressive strength	46.2 MPa
Fracture energy, G_F	147.6 N/m
Flexural tensile strength, f_{ff}	4.4 MPa

3 EXPERIMENTAL TECHNIQUES

The quasi-static tests have been performed using a servo-controlled universal machine. Other tests at medium and high strain-rates have been carried out using the following techniques:

3.1 Hydro-pneumatic device for small specimen

The tests in the range of 10^{-2} – 10^{-3} s⁻¹ on cubes side 60 mm were carried out by means of a hydro-pneumatic device developed at the JRC. The device can be set to perform either at constant strain rate or at constant stress. For a test at a constant strain-rate water is put into the upper tank of the device, and both chambers are loaded at an equal pressure; after the membrane has been punctured, the liquid flows out through a calibrated orifice at constant strain-rate, thus imposing a strain on the specimen. The pressure acting on the piston governs the displacement velocity, because the pressure load is greater than the force needed for breaking the specimen.

The scheme of the device is shown in Figure 1.

The displacements of the specimen ends were recorded by means of an opto-electronic device. The mean strain was obtained by dividing the difference between the end displacements by the specimen length.

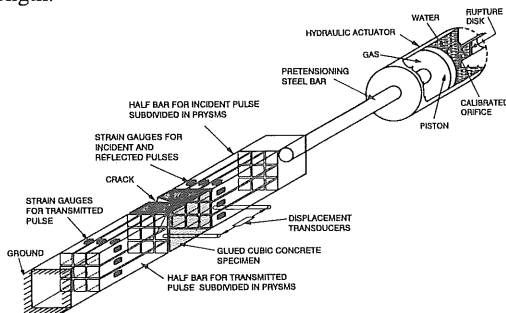


Figure 1. Hydro-pneumatic device for small specimens.

3.2 Hydro-pneumatic device for large specimen

The tests were carried out using the Bar Bundle connected to hydro-pneumatic device. The medium and low strain-rate tests were conducted by means of

a command device with a cylinder that can produce a tensile or compressive pressure effect under control by a valve; the calibration of this valve has a linear variation in time. The linear increasing velocity is characterized by governing flow (manual setting) that permit to obtain constant capacity sufficient to realize the established value of load increment in the time.

The limits of this device are 500 kN in 0.25 s in tension and 500 kN in about 250 s.

3.3 High Strain-rate tests

The Hopkinson Bar Bundle (HBB) has been developed and installed in the Large Dynamic Testing Facility (LDTF) of the Joint Research Centre at Ispra (see Figure 2). The HBB is a special equipment that enables precise measurement of the stress-strain diagram, including the softening branch, which is important for the correct evaluation of the energy absorption capability of plain concrete used in civil engineering structures. The HBB system consists of two bundles of 25 aluminum smaller bars, to each of which the concrete test specimen is glued using an epoxy resin. Using this technique concrete specimens with square cross section of 200 x 200 mm² were tested. Strain gauges on each individual bar in the bundles enables measurement of the incident, reflected and transmitted pulses on each portion of the concrete specimen cross-section demarcated by each aligned pair of bars in the two bundles.

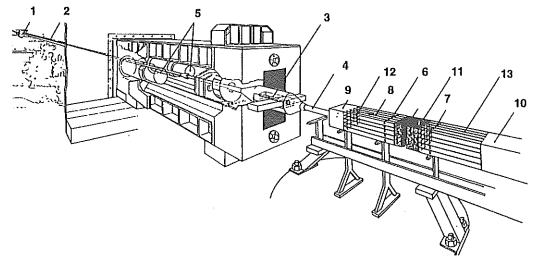


Figure 2. Experimental set-up: 1. hydraulic actuator; 2. high strength steel cables for energy storage (100 m); 3. explosive bolt; 4. loading bar; 5. hydraulic dampers; 6. strain gauges to measure incident and reflected pulses; 7. strain gauges to measure transmitted pulses; 8. load direction; 9. instrumented input solid aluminum bar; 10. instrumented output solid aluminum bar; 11. specimen; 12. elementary input bar bundle; 13. elementary output bar bundle.

A test with the LDTF-HBB is performed as follows:

- a hydraulic actuator, of maximum loading capacity of 5 MN, is used to pull 32 cables of high strength steel having a length of 100 m; the pretension stored in these cables is resisted by one

grounded explosive bolt in the blocking device (see Figure 2);

- the second operation is the rupture of the explosive bolt which gives rise to a tensile mechanical pulse of 40 ms duration with linear loading rate during the rise time, propagating along the Hopkinson bar bundle and bringing to fracture the plain concrete specimen.

The application of the uniaxial propagation theory of elastic stress waves along bars having small transverse dimensions with respect to the wavelength of the applied stress pulse allows the calculation of the following quantities (Davies 1948, Lindholm 1971).

- History and amplitude $P(t)$ of the loading pulse generated by the pretensioned bar and propagated towards the specimen along the incident (input) bar

$$P(t) = A_I \cdot E_I \cdot \epsilon_I(t) \quad (1)$$

where: t = time; A_I = Input bar cross section area; E_I = elastic modulus of the input bar; $\epsilon_I(t)$ = elastic strain of the input bar caused by the incident pulse.

- History and amplitude of loading $R(t)$ at both ends, connected to the specimen, of the incident and transmission bars.

$$R_{input} = A_I \cdot E_I \cdot [\epsilon_I(t) + \epsilon_R(t)] \quad (2)$$

$$R_{output} = A_O \cdot E_O \cdot \epsilon_T(t) \quad (3)$$

where: A_O = Output bar cross section area; E_O = elastic modulus of the output bar; $\epsilon_R(t)$ = elastic strain of the input bar caused by the reflected pulse; $\epsilon_T(t)$ = elastic strain of the output bar caused by the transmitted pulse.

- History and amplitude of displacement $S(t)$ at both ends, connected to the specimen, of the input and output bars

$$S_{input}(t) = C_0 \int [\epsilon_I(t) - \epsilon_T(t)] dt \quad (4)$$

$$S_{output}(t) = C_0 \int [\epsilon_T(t)] dt \quad (5)$$

where C_0 is the bar elastic uniaxial wave speed

The HBB bar system satisfies the condition of applicability of the uniaxial elastic wave propagation theory because the pulse wavelength (100m) is much higher than the transversal length of the bar (~0.3 m). Therefore, whatever the length of specimen inserted between the input and output bars, the modified Hopkinson's bar equipment described can be considered as a transducer system which allows the

measurements of the load-displacement characteristic of the specimen by exerting strict control over the stress wave propagation.

Finally, when the specimen is short, so that the travel time of the elasto-plastic wave through the specimen is small in comparison to the duration of the test, the specimen can be considered as being in load equilibrium at its ends, and in homogeneous stress state created by many wave reflections taking place at the ends (interfaces specimen-bars) of the specimen. These last experimental conditions constitute the basic assumptions in order to calculate the average stress-strain characteristics of the specimen material at different strain rates, which are given by the following equations:

- Stress

$$\sigma(t) = E \frac{A}{A_s} \epsilon_T(t) \quad (6)$$

- Strain

$$\epsilon(t) = -\frac{2C_0 \int_0^t \epsilon_R(t) dt}{L_s} \quad (7)$$

- Strain rate

$$\dot{\epsilon}(t) = -\frac{2C_0}{L_s} \epsilon_R(t) \quad (8)$$

where: A_s = specimen cross section area and L_s = specimen length.

4 EXPERIMENTAL RESULTS

The experimental results on small size concrete cubic (60 mm side) specimens have been obtained using different testing methods for the different cases of loading rate. They were: Hopkinson bar technique for the impact case; Hydro-pneumatic device for the earthquake one and the direct tensile test (universal machine) for the quasi-static case. The results obtained at the high, medium and quasi-static strain-rate are summarized in Table 2.

The results of the experiments carried out on concrete specimens (cube 200 mm side, 25 mm maximum aggregate size) cured at three different curing conditions and tested at three strain rates are reported in Table 3.

The increase of the tensile strength with increasing relative humidity (Cadoni et al. 2001) inside the concrete is clearly observed for impact loads (Tab. 3). A slight decrease of tensile strength is instead noticed for saturated concrete specimens under quasi-static loads. Furthermore, these results show that different levels of free water inside the specimen have an important influence on the sensitivity

Table 2. Strain-rate effect on tensile strength in two different materials (5 and 10 mm maximum aggregate size) on cubic specimens 60 mm side.

Type of loads	Strain rate [s ⁻¹]	Tensile Strength (max aggr. size 5 mm) [MPa]	Tensile Strength (max aggr. size 10 mm) [MPa]
Hard Impact	10	11.8	10.5
Soft Impact	1	9.2	7.4
Earthquake	10 ⁻²	2.5	4.4
Quasi-Static	10 ⁻⁶	2.7	3.6

Table 3. Strain-rate effect on the tensile strength of the concrete cured at three different curing conditions

Type of loads	Strain rate [s ⁻¹]	Tensile Strength		
		Specimens drying at 50°C [MPa]	Specimens 20°C-50% R.H. curing [MPa]	Specimens saturated [MPa]
Hard Impact	10	5.16	6.56	9.26
Soft Impact	1	4.03	5.51	6.70
Quasi-Static	10 ⁻⁶	3.28	3.53	3.03

of the concrete response to the strain-rate.

All the average results (Cadoni et al. 2000) are summarized in Figure 3, where the ratio of maximum tensile strength at high strain rate to quasi-static maximum tensile strength is shown in function of the strain-rate. It must be considered that these results include size effect (caused by different size of cubes and different aggregate size) and regard specimens with standard curing conditions (95% R.H., 20°C). In Figure 4 the comparison between two stress vs. strain curves is shown.

In Table 4 are shown the results obtained with plain concrete with 10 mm maximum aggregate size. These data describe the variation of the mechanical characteristic as a function of the strain rate. The specimen were cubic 60 mm side. The values of strain, stress, elastic modulus and specific fracture energy increase with the strain-rate. This fact means that at high strain rate the material increase its absorption capability.

5 FRACTURE PROCESS OF PLAIN CONCRETE AT HIGH LOADING RATE

It is well known from the literature (Reinhardt 1982, Rossi et al. 1982) that the mechanical properties of concrete are strain-rate dependent so that the strength is higher at high loading rates. One important reason is the fracture phenomenon: in the static case the cracks follow the weaker aggregate-mortar

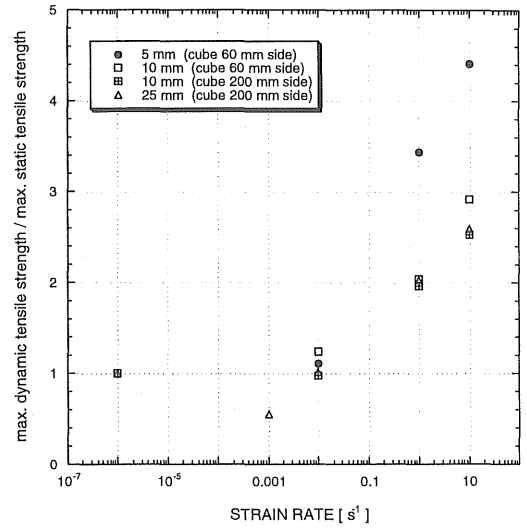


Figure 3. Strain-rate effect on max. tensile strength in three different materials

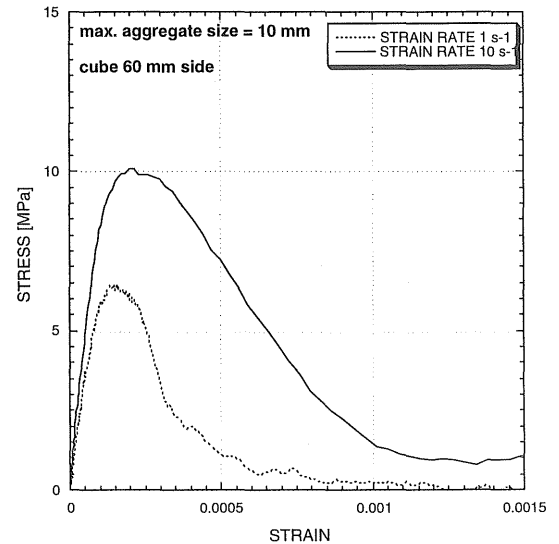


Figure 4. Stress vs. strain curves for two strain-rates

Table 4: Mechanical characteristic variation of plain concrete with 10 mm maximum aggregate size measured on cubic specimens 60 mm side.

Type of loads	Strain rate [s ⁻¹]	Tensile strength [MPa]	Max. strain [%]	Elastic modulus [GPa]	Fracture energy [N/m]
Hard Impact	10	10.52	236	76.7	397
Soft Impact	1	7.37	163	59.5	89
Quasi-Static	10 ⁻⁶	3.61	-	37.3	68

interface; in the dynamic case the cracks propagate also through the hard aggregate. Another aspect is that in the dynamic case it is normally not just one crack present; often many cracks are activated. For these reason a local analysis of the specimen is essential and the HBB technique provides an answer to this necessity.

During the fracturing process each Nth pair of specular bars of the two bundles, which are individually instrumented with strain gauges, measure the incident, reflected and transmitted pulses σ_{IN} , σ_{RN} , σ_{TN} , only in the portion of the specimen cross-section facing the cross-sections of this particular pair.

It is postulated that during the fracturing process each pair of the specular bars of the bundles will be in one of the following physical situations (Albertini et al. 1999):

- Facing an uncracked portion of the specimen cross-section, therefore measuring a relatively small reflected pulse σ_{RN} and a large transmitted pulse σ_{TN}
- Facing a semi-cracked portion of the specimen cross-section, therefore in the measurement situation where σ_{RN} is strongly increasing and σ_{TN} strongly decreasing
- Facing a totally cracked portion of the specimen cross-section, therefore measuring a reflected pulse σ_{RN} of equal amplitude and of opposite sign to the incident pulse σ_{IN} , while the correlated transmitted pulse decreases to $\sigma_{TN} = 0$

In the following analysis, the beginning of the fracturing process has been considered to be the moment at which the first of the bars of the bundle shows the maximum load of the portion of the specimen cross-section facing it. In other words, the concrete part facing the Nth bar of the bundle begins to fracture when the corresponding transmitted pulse σ_{TN} reaches its maximum and begins to decrease. Figures 5 and 6 compare the time instants and the locations (bars of the bundle) on the specimen cross-section in which σ_{TN} reaches its maximum, with the total load value. From this correlation established in Figures 5 and 6 it can be seen that the fracturing process begins in the ascending branch of the total load resisted by the specimen; the total load in Figures 5 and 6 has been measured on the whole bar and as a sum of the loads on the bars of the bundle. Interesting correlation is also possible by comparing the stress-strain diagrams obtained from each bar pair of the bundle with the morphology of the corresponding part of the specimen cross-section (e.g. mix percentages of mortar and aggregates). From this analysis it can be seen that:

- the initiation of the first crack at 121 μs corresponds to the beginning of the loss of linearity of the

ascending branch of the total loading;

- in ten microseconds the crack initiation spreads over the whole specimen cross-section revealing the multi-activation mode of the fracture process;
- the spread time of the crack initiation over the whole cross-section (from 121 to 131 μs) corresponds to the beginning of the total loading softening branch.

Taking into account the last observations it is possible to define a more refined analysis method for the construction of the true stress-strain diagram starting from the bar bundle records. This refined method introduces for each elementary bundle bar an evaluation of the residual resisting cross-section A_{TRUE} of the Nth facing part of the concrete specimen by decreasing the initial value A_0 by an amount which takes into account the separation due to the crack propagation.

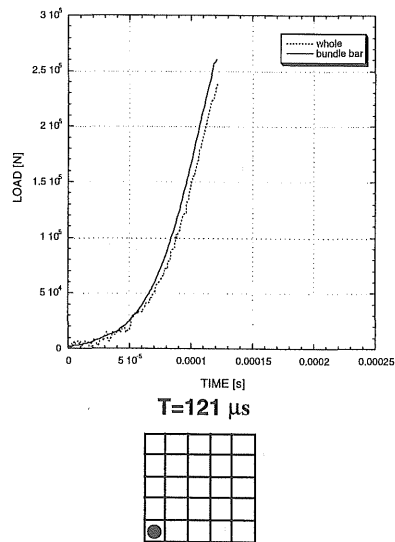


Figure 5. Total load vs. time curves of the bundle bar and whole bar compared with crack initiation when $\sigma_{TN} = \text{max}$

The cracking process of concrete subjected to tensile loading is normally described using a fracture mechanics approach. The behavior in tension can be represented by different phases. First of all it must be recalled that due to shrinkage of the matrix restrained by the aggregate in the material, micro-damage is present. It is possible to find micro-cracks with the same probability in all volume elements because they are randomly distributed. When the stress increases, these micro-cracks grow and crack localization take place, forming some macro-cracks. Finally, the macro-cracks propagate leading to failure the specimen.

When the strain-rate is increased from 1 s^{-1} to 10

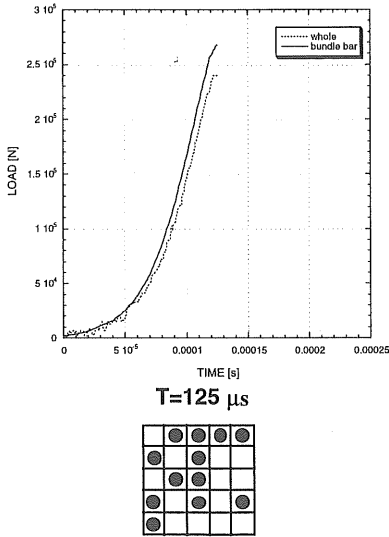


Figure 6. Total load vs. time curves of the bundle bar and whole bar compared with crack initiation when $\sigma_{TN} = \max$

s^{-1} the stress wave propagation effects on the cracking process changes must be considered; in fact, while in the static case the crack chooses the way with the minimum energy requirement (i.e. matrix-aggregate interfaces), in the dynamic one the wave propagation also induces cracking in the tougher aggregate. Using the information obtained from the bundle bar it is possible to describe the mode and the growth of the fracture through the cross-section of the specimen.

The fracture propagation has been represented by means of diagrams in which the positions of cracks at successive times on the specimen cross-section have been indicated by iso-chrono curves. In Figures 7 and 8 the crack propagation is shown for two tests at 10 and $1 s^{-1}$ respectively, where the iso-chrono curves of the positions of the cracks during the fracture process are indicated. It can be observed that in the case of impact load (Fig. 7) there is not a unique crack starting and growing from a single point but there are many macro-cracks starting simultaneously and propagating from many points; in other words the multiactivation of cracks is present.

The multiactivation of cracks leading to fracture is also confirmed by the observation from Figure 7 that in the very short time of about $20 ms$ the crack initiation is spread all over the specimen cross-section.

The multiactivation of fracture is an effect of the impact loading. Cracks are growing so rapidly and are so well distributed over the specimen cross-section that all material particles are accelerated by the pulse and there is no time to concentrate the load only on the weakest place; many weak points are

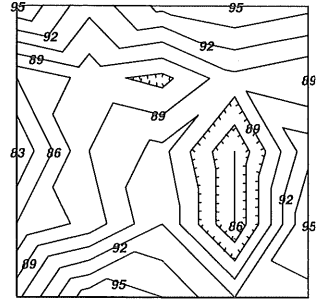


Figure 7. Crack propagation of specimen (concrete with $25 mm$ maximum aggregate size) at strain-rates $10 s^{-1}$.

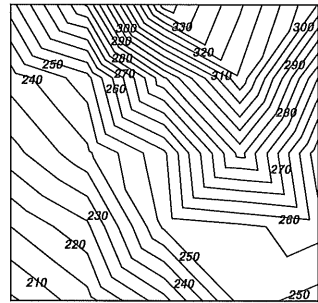


Figure 8. Crack propagation of specimen (concrete with $25 mm$ maximum aggregate size) at strain-rates $1 s^{-1}$.

simultaneously brought to fracture by the load wave. In the tests carried out at strain-rate of $1 s^{-1}$ (Fig. 8) is evident that a single crack propagates through the cross section, and the cracking process takes about $50 \mu s$ to cover the entire cross section.

6 CONCLUSIONS

The study of the dynamic tensile behavior of concrete, that falls within a broader experimental campaign, has been performed to answer the necessity to give guidelines for the design of impact resistant concrete structures and to establish realistic material models to be implemented in numerical computational codes.

The quantity of experimental results obtained is very large. In this paper some global results have been presented. Observations of the phenomena arising from high strain rate loading can be summarized as follows:

- The mechanical properties of the tested plain concrete show a strain-rate dependence consisting in an increase of strength, ductility and energy absorption capability with increasing strain-rate.
- The increase of strength, ductility and energy absorption is non linear and becomes remarkable at

strain-rates where stress wave propagation begins to be the mode of loading the specimen ($>1s^{-1}$).

REFERENCES

- Albertini, C. & Montagnani, M. 1994. Study of the true tensile stress-strain diagram of plain concrete with real size aggregate; need for and design of a large Hopkinson bar bundle, *Journal de Physique IV*, 4, C8.
- Albertini, C., Cadoni, E., & Labibes, K. 1997. Impact fracture process and mechanical properties of plain concrete by means of an Hopkinson bar bundle, *Journal de Physique IV*, 7, C4, 915-920.
- Albertini, C., Cadoni, E. & Labibes, K. 1998, Mechanical characterization and fracture process of concrete at high strain-rates, in O.E. Gjrv, K.Sakai N.Banthia eds. *Concrete under severe conditions*, Vol. 2, E&FN SPON, 735-744.
- Albertini, C., Cadoni, E., & Labibes, K. 1999, Study of the mechanical properties of plain concrete under dynamic loading, , *Experimental Mechanics*, 39, 137-141.
- Davies, R.M. 1948. A Critical Study of the Hopkinson Pressure Bar, *Phil. Trans.Roy. Soc.*, London, Ser. A, 240-375.
- Cadoni, E., Labibes, K., Albertini, C., Berra, M. & Giangrasso M.. Strain-rate effect on concrete with different level of the relative humidity, *Materials and Structures*, Vol. 34, N. 235, 2001, pp. 21-26.
- Cadoni, E., Labibes, K., Berra, M., Giangrasso, M. & Albertini, C., High strain-rate tensile concrete behaviour, *Magazine of Concrete Research*, vol. 52, No.5, Oct., pp. 365-370.
- Lindholm, U.S. 1971. *High Strain Rate Test*, Technique of Metals Research (Wiley), Vol. 5 Part. 1.
- Reinhardt, H.W. 1982. Concrete under impact loading. Tensile strength and bond, *Heron*, 27, (3).
- Rossi, P., Van Mier, J.M.G., Boulay, C. & Le Maou F. 1982. The dynamic behaviour of concrete: influence of free water, *Materials and Structures*, 25, 509-514.